Designing Nanogadgets by Interconnecting Carbon Nanotubes with Zinc Layers

Mohammad Khazaei,[†,*] Sang Uck Lee,[†] Fabio Pichierri,[‡] and Yoshiyuki Kawazoe[†]

[†]Institute for Materials Research, Tohoku University, 2-1-1 Katahira, Aoba-ku, Sendai 980-8577, Japan, and [‡]G-COE Laboratory, Department of Applied Chemistry, Graduate School of Engineering, Tohoku University, Aoba-yama 6-6-07, Sendai 980-8579, Japan

ABSTRACT Using first-principles calculations we propose a new approach for the design of functional units obtained by interconnecting carbon nanotubes (CNTs) with different numbers of zinc layers. The theoretical investigations on electron transport properties of the resulting 1D heterojunctions containing CNTs with same or different chiralities (*i.e.*, metallic or semiconducting) and one, two, or three zinc layers illustrate that the junctions with two semiconducting CNTs show semiconducting *I*—*V* characteristics while the junctions with two different CNT electrodes (metallic and semiconducting) show rectifying diode properties. The remarkable features emerging from this study is that the zinc layers behave as a momentum filter (near the Fermi energy the Bloch states having the same orbital character as the molecular states conduct well) when they are inserted within metallic CNT electrodes thereby providing 1D heterojunctions that can act as a wire-like, negative differential resistance (NDR), or varistor-type nanoscale device. Our results prove the idea that it is possible to design specific heterojunctions, which can select a conducting channel between two electrodes. Also, it is worth mentioning that in this study for the first time we have designed a nanoscale device with the characteristics of a varistor.

KEYWORDS: carbon nanotubes · electron transport · wire · negative-differential resistance · varistor · rectifying diode

Advances in the synthesis of hybrid organic—inorganic materials are paving the way toward the discovery of novel physical properties, which can be exploited in a number of nanotechnology applications. A particularly important group of hybrid nanomaterials is that of 1D nanoscale heterojunctions, which represent the key elements for the fabrication of different nanoscale electronic devices (*i.e.*, nanogadgets) such as nanodiodes and nanosensors.[1] Because experimentally exploring large numbers of combinations of organic and inorganic materials is both time-consuming and economically expensive, computer-aided design and first-principles atomic-scale simulations are tools of paramount importance in the hand of researchers.[2] In this regard, we have recently investigated the structures and electron transport properties of organic 1D heterojunctions obtained by interconnecting carbon nanotubes (CNTs) with peptide linkages.[3,4] On the basis of results obtained from a series of Green's function calculations we predicted that the heterojunction made of two different CNT units, that is, one metallic and the other semiconducting, behaves like a rectifying diode.

Although chemical functionalization of CNTs has progressed significantly in the recent years,[5–7] one of the requirements for the realization of semirigid junctions is that several linkages (*e.g.*, five in our peptide-CNT models)[4] should be attached to the nanotubes' mouths. Hence, the possibility of interconnecting pristine CNT using metals is appealing for it might considerably simplify the fabrication process while providing nanoscale devices with more rigid junctions as well as novel physical properties. For instance, one of us (F.P.) has recently proposed connecting *thia*-cucurbituril macrocycles with transition metal ions such as Pd(II), Pt(II), and Hg(II) to fabricate modular nanotubes of controllable dimensions.[8]

In this study, using first-principles calculations we have designed and investigated the electron transport properties of novel 1D heterojunctions obtained by connecting layers of Zn atoms to two CNTs with same or different chiralities. The use of zinc is motivated by its abundance (76 ppm of the Earth's crust) which is similar to that of copper (68 ppm)[9] and the highly developed synthetic chemistry methods for the preparation of organometallic compounds containing Zn—C bonds.[10] Also, the existence of two stable oxidation states, Zn^{2+} and Zn_2^{2+}, offers the possibility of tuning both the structural and electronic properties of the resulting Zn-containing heterojunctions.[9] Heterojunctions based on CNTs and metals are expected being more robust than the flexible all-organic heterojunctions containing peptide linkages that we have recently investigated.[4] Our transport results show that in these Zn-based

*Address correspondence to khazaei@imr.edu.

Received for review December 21, 2007 and accepted April 24, 2008.

Published online May 10, 2008.
10.1021/nn7004377 CCC: $40.75

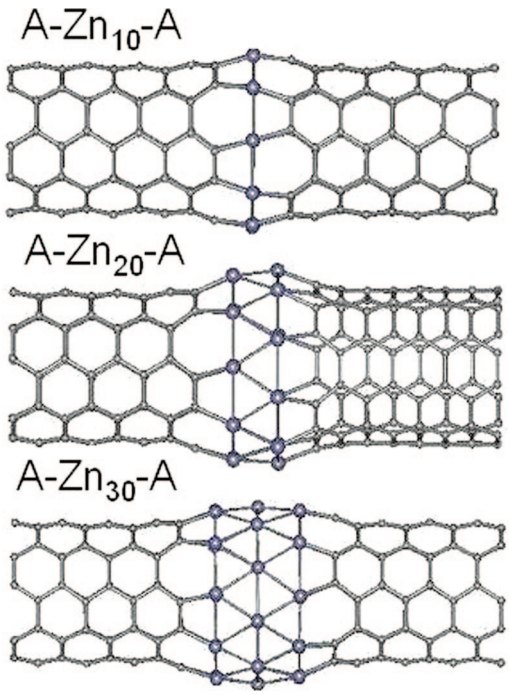

Figure 1. Model junctions made from two armchair (5,5) nanotubes interconnected with different numbers of zinc layers.

heterojunctions the number of metal layers controls the functionality of the designed junction. In other words, by adjusting the number of Zn layers between the nanotubes, we are able to design nanoscale devices embodying different functionalities, such as quantum wire-like conductance, negative-differential resistance (NDR), varistor-like, and rectification.

RESULTS AND DISCUSSIONS

To show how functionalities of zinc-nanotube junctions are controlled by the presence of zinc layers, we have prepared nine different heterojunction models. The junctions consist of different numbers of zinc layers (one, two, three zinc layers containing 10, 20, and 30 zinc atoms, respectively) sandwiched between two CNTs. In six model junctions, the interconnected CNTs are purely metallic ((5,5) armchair) or semiconducting ((10,0) zigzag), while in the remaining three heterojunctions, one of the CNTs is metallic and the other one is semiconducting. Although we have performed the transport calculations for all of the nine designed junctions, we will discuss in detail three model junctions with metallic CNT electrodes, A-Zn_{10}-A, A-Zn_{20}-A, and A-Zn_{30}-A (A = armchair, see Figure 1), since their $I-V$ characteristics shown in Figure 2 are among the most interesting cases characterized by wire-like, NDR, and varistor-type behaviors. We will comment on the other six junctions briefly at the end.

To better understand the current characteristics of the model junctions shown in Figure 2, we have considered their corresponding total transmission curves at different applied voltages, 0.0, 1.0, and 1.5 V, depicted in Figure 3. From Figure 3, it is observed that at all applied voltages there are always some electron transmissions near the Fermi energy resulting in metallic behavior of A-Zn_{10}-A, A-Zn_{20}-A, and A-Zn_{30}-A. Figure 3A shows that the broadening of the peak located between 1.2 and 2.2 eV decreases at high voltages, and a new peak appears above the Fermi energy around 1.0 eV. To consider the above behavior, we have analyzed the energy shift of the molecular states of A-Zn_{10}-A (device part only) that are involved in the transmission. To this end the self-consistent Hamiltonian is projected onto the junction's orbitals, then the so obtained sub-Hamiltonian matrix is diagonalized.[11,12] Figure 4 shows the energy shift of the obtained molecular projected self-consistent Hamiltonian (MPSH) states of A-Zn_{10}-A labeled 300−330 whose energies are in the range from −2.0 to 2.0 eV at the different applied voltages. For example at zero voltage the corresponding energy of the MPSH state number 315 (shown by a dotted line in Figure 4) is 1.2 eV. From the energy evolution of the MPSH state 315, it is clearly seen that its energy is shifted to lower energies by increasing the applied voltages; the color changes from yellow to red. Figure 4 shows that under applied voltages, the MPSH states above the Fermi energy are shifted to lower energies resulting in a decreased peak broadening at 1.2−2.2 eV and a new peak appears around 1.0 eV. By performing the same analysis for A-Zn_{20}-A and A-Zn_{30}-A (not shown), it can be explained why under applied voltages the peaks in the corresponding transmission curves are shifted to lower energies, as shown in Figure 3B,C. Let us now investigate the transmission curves of A-Zn_{20}-A and A-Zn_{30}-A in more detail.

Figure 3 panels B and C show that the electron transmissions near the Fermi energy are very much pronounced in comparison to those in Figure 3A. Also, a

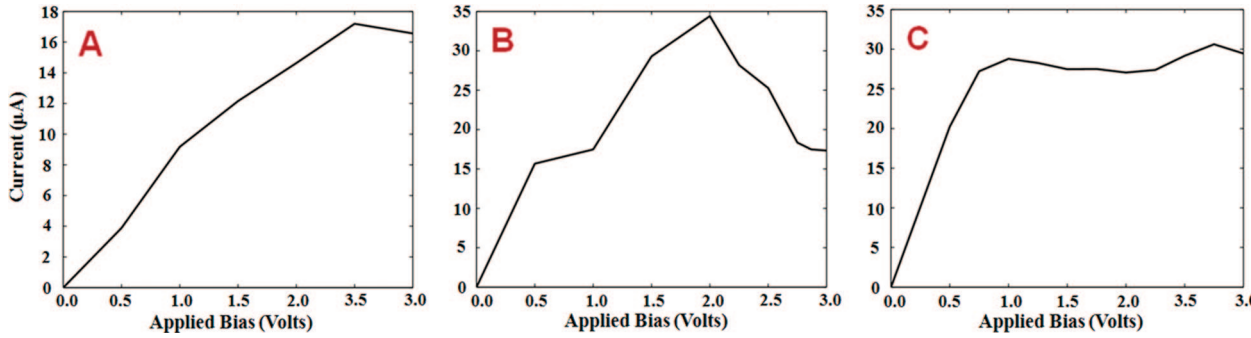

Figure 2. Panels a, b, and c are the $I-V$ characteristics of model junctions A-Zn_{10}-A, A-Zn_{20}-A, and A-Zn_{30}-A, respectively.

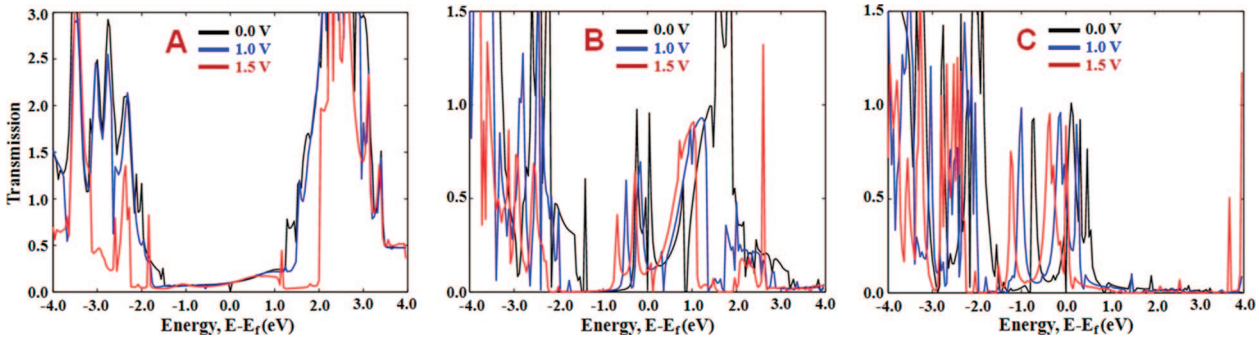

Figure 3. Panels a, b, and c are the total electron transmission curves of model junctions A-Zn$_{10}$-A, A-Zn$_{20}$-A, and A-Zn$_{30}$-A, respectively.

large gap appears in the transmission curves of junctions A-Zn$_{20}$-A (at ~3.0 eV) and A-Zn$_{30}$-A (at ~1.0 eV), which is not seen in A-Zn$_{10}$-A. From Figure 3B,C it is seen that the transmission coefficients of many of the states whose energies are between −1.0 and 1.0 eV are ~1.0. This means that those states are completely delocalized throughout the device part. Recent studies performed by Kaun *et al.* indicated that only those Bloch bands having the same orbital character as the MPSH states near the Fermi energy conduct well.[12] This characteristic makes the system to behave like a momentum filter because only those incoming states with matched character to the junction can conduct efficiently.[12] In this regard, to explain why a gap appears above the Fermi energy and why some of the states between −1.0 and 1.0 eV are completely delocalized throughout the above junctions, we also analyzed the characteristics of their molecular orbitals (see Supporting Information). Our analysis indicates that near the Fermi energy there are significant contributions from p_x and p_y orbitals rather than s and p_z orbitals. This is similar to the case of pristine armchair and zigzag nanotubes both of which have p_x and p_y characters near the Fermi energy between −4 to 4 eV. When we increase the number of zinc layers, from one to three, the contribution of the p_x and p_y orbitals improves, that is, a better delocalization of the states is observed in the transmission curves particularly at the Fermi energy. This is the reason why near the Fermi energy some of the MPSH states show perfect delocalization (transmission ~1.0) due to the similarity of their orbital characteristics to the Bloch states of the electrodes. From the comparison between the orbital characteristics and the transmission curves (computed at zero voltage), we found that the gaps appear at the energies where the contribution of d-type orbitals (d_{z^2}, d_{xz} d_{yz} $d_{x^2-y^2}$ and d_{xy}) in the corresponding conducting channels is comparable with the contribution of s and p-type orbitals. When the contribution of d-type orbitals increases, the molecular states become mainly localized on the zinc layers resulting in less delocalization of the states along the junction. We expect that if we increase the number of zinc layers (≥4) a gap would appear at the Fermi energy as a result of the increased d-type orbital character.

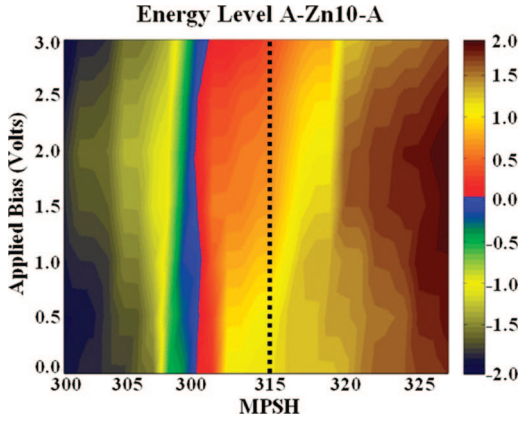

Figure 4. The energy shift of the molecular projected self-consistent Hamiltonian (MPSH) states of A-Zn$_{10}$-A near the Fermi energy under different applied voltages. The vertical color bar is for the energy of MPSH states. The black dotted line is a guide for the eyes that shows how the energy of a MPSH state changes by applied voltages. The interface between red and blue colors shows the position of the Fermi energy (0.0 eV).

To explain the wire-like behavior of A-Zn$_{10}$-A, NDR property of A-Zn$_{20}$-A, and varistor-type characteristic of A-Zn$_{30}$-A, we have plotted the total transmission spectra of the designed junctions under various bias voltages, namely from 0.0 to 3.0 V as shown in Figure 5. From this figure it is observed that the intense transmission peaks near the Fermi energy (shown by white arrows) are shifted to lower energies by increasing the applied voltages. In Figure 5, the white dotted lines indicate the range of integration window that is used to calculate the conducted current through the junction at each applied voltage. From Figure 5A, it is observed that although there are some intense peaks above the Fermi energy, none of them enters into the integration window. Just the transmission amplitude of the states near the Fermi energy increases slowly by increasing the applied voltage. Therefore A-Zn$_{10}$-A shows metallic wire-like performance with typical ohmic resistance behavior. Let us now analyze the current response of A-Zn$_{20}$-A and A-Zn$_{30}$-A to the applied voltages.

From Figure 5B,C, it is observed that there are two intense peaks available near the Fermi energy. At zero voltage, from the transmission spectra of A-Zn$_{20}$-A, Figure 5B, it is observed that one of the peaks has been located near the Fermi energy level while the other one lies above the Fermi energy at around 1.5 eV. It is also observed that the latter peak enters into the integration window

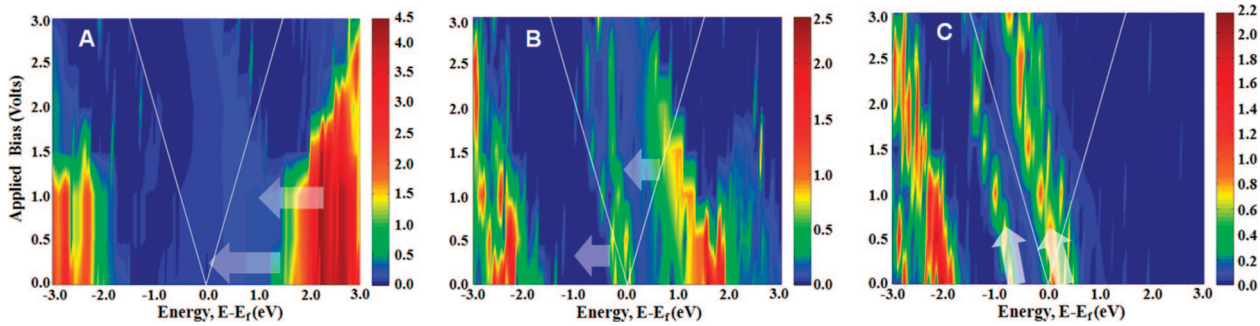

Figure 5. Panels a, b, and c are the total electron spectra of model junctions A-Zn$_{10}$-A, A-Zn$_{20}$-A, and A-Zn$_{30}$-A, respectively. The vertical color bar is for the values of transmission. The white dotted lines indicate the integration window in transport calculations at different applied voltages. The white arrows show how the intense transmission peaks near the Fermi energy are shifted at different applied voltages.

at 1.0 V. This is the reason why at voltages larger than 1.0 V, the current increases strongly, see Figure 2B. However the current does not always increase by increasing the applied voltage. Figure 5B shows that while the peaks are shifted to lower energies, their amplitudes decrease. Hence at voltages larger than 2.0 V, the current decreases resulting in NDR characteristic of A-Zn$_{20}$-A. In devices displaying NDR characteristics, the decrease in current is caused by an increase in voltage above a certain threshold. NDR property is highly desired in switching devices.

From Figure 5C, it is seen that similar to A-Zn$_{20}$-A, in the transmission spectra of A-Zn$_{30}$-A, there are two intense peaks above and below the Fermi energy. It is observed that by applying external voltages, the peaks are shifted downward. Hence the peak, which is above the Fermi energy, enters into the integration window upon applying small voltages. The $I-V$ characteristic of A-Zn$_{30}$-A shows varistor-type behavior (*i.e.*, a resistor with a significantly nonohmic current−voltage characteristic) because the amplitude and number of conducting channels, which are located in the integration window, are constant for a large range of applied voltages (from 1.0 to 3.0 V). There exists a very small increase of current at 2.75 V, as seen in Figure 2C, because the transmission peak which is under the Fermi energy enters the integration window at voltages larger than 2.5 V, see Figure 5C. However it disappears soon above 2.75 V. It is interesting to mention that the most common type of varistor is that made of metal oxides. These varistors contain a mass of zinc oxide grains, in a matrix of other metal oxides, sandwiched between two metal plates (the electrodes).[13] The varistors are often used to protect circuits against excessive voltage.

Our quantum transport calculations show that the junctions made of two semiconducting carbon nanotubes interconnected with zinc layers, Z−Zn$_x$−Z (Z = zigzag, x = 10, 20, 30), display semiconducting $I-V$ characteristics resulting from the intrinsic properties of (10,0) semiconducting carbon nanotube electrodes with a gap at the Fermi energy. Also, the results show that the threshold voltage in model junctions with semiconducting CNT electrodes increases from 0.5 to 1.25 V when the number of layers increases from one to three. It is observed that the amount of conducted current decreases significantly by increasing the number of zinc layers due to an increase in d-type orbital character of the molecular orbitals near the Fermi energy (see Supporting Information).

Also, our calculations indicate that the model junctions made of different nanotube electrodes, semiconducting and metallic, show rectifying diode properties. Interestingly, the junction with two zinc layers shows better rectifying property in comparison to the junctions containing one and three zinc layers. It is worth mentioning that by comparing the transmission spectra of the systems herein investigated, we found that the transmission behavior of Z−Zn$_x$−A (x = 10, 20, and 30) junctions at positive voltages (electrons are injected from the zigzag electrode) is similar to that of A−Zn$_x$−A junctions while at the negative voltages (electrons are injected from the armchair electrode) the transmission behavior is similar to that of Z−Zn$_x$−Z junctions though the intensities of the peaks are lower. This result is a consequence of the electronic structure of the electrode that receives the injected electrons. Interestingly, we have seen the above behavior also for the carbon nanotubes interconnected with peptide linkages.[4]

CONCLUSION

Interconnecting CNTs with different numbers of metal atoms (here we used Zn atoms) paves the way toward the design of nanogadgets embodied with rectifying, NDR, varistor-like, or wire-like characteristics. The atomic structures of the resulting 1D heterojunctions were determined using first-principles total energy calculations. Subsequently, their electron transport properties were examined using the nonequilibrium Green's function formalism in combination with density functional theory. Our calculations show that the shift of the molecule's projected self-consistent Hamiltonian (MPSH) states under applied voltages, and the similarities between the orbital characteristic of MPSH states and the orbital characteristics of extended Bloch states provided by semi-infinite nanotubes, result in the differ-

ent electronic characteristics of the designed junctions. Although there are many possible ways for interconnecting CNTs together like using organic linkages, our study indicates that the use of transition metals provides more possibilities for the development of novel nanoscale devices. In this regard, we have designed the first nanoscale device displaying varistor-like behavior, which has not been as yet observed in the case of all-organic homo- and heterojunctions.

COMPUTATIONAL APPROACH

In general, when two CNTs are joined together with either metal−carbon or covalent-type linkages, one of the CNTs rotates in the direction opposite to the other one.[3,4] This axial rotation arises from the adjustment of the linkage atoms, which adapt themselves to the geometry of the CNTs. Following these considerations, we prepared our Zn-CNT models provided with short CNT segments (six carbon layers) and fully optimized their geometries before performing any transport calculation. In our designed models, the zinc atoms join the inner mouths of the interconnected CNT segments and hydrogen atoms saturate the outer mouths of CNTs. The calculations are *ab initio* based on the generalized gradient approximation (GGA) of density functional theory (DFT). The exchange-correlation functional of GGA is parametrized by Perdew and Wang (PW91).[14] The interaction between the ions and electrons are described by ultrasoft Vanderbilt pseudopotentials. We use a plane-wave (PW) basis set for the expansion of the electronic states. The number of plane-wave basis functions is determined by a cutoff energy of 250 eV. All the geometrical optimizations are performed with the Vienna *ab Initio* Simulation Package (VASP).[15] The conjugate gradient method is used to optimize all the models. The convergence criteria adopted here assumes that the maximum force acting on each atom in the relaxed structure is less than 0.04 eV/Å.

To study the transport properties of the proposed junctions, we implement some two-probe systems, "electrode−device−electrode", from the optimized junctions. Those systems are obtained first by detaching the terminal CH moieties from the CNT ends of the optimized model junctions and then by connecting the left and right sides of the junctions to appropriate semi-infinite CNT electrodes. To achieve maximum coupling between the junctions and the electrodes, the chiralities of the latter are the same as those of the former. To simulate the electron transport of the proposed junctions, a set of calculations is carried out using the nonequilibrium Green's function combined with DFT at the finite biases. The DFT calculations are based on the GGA and the exchange-correlation functional of Perdew−Burke− Ernzerhof.[16] The core−electrons are represented by improved Troullier−Martins pseudopotentials,[17] whereas the valence electrons are described by a numerical atomic orbital basis set of double-ς type. All the transport calculations are performed using Atomistix ToolKit (ATK) software package (version 2.0.4). The above software package has the ability to model the transport properties of nanoscale devices that consist of an atomic-scale device coupled to heterobulk systems, or electrodes. More details on the method employed here can be found in refs 18 and 19.

Acknowledgment. The authors sincerely thank the crew of the Center for Computational Materials Science of the Institute for Materials Research, Tohoku University, for their continuous support of the supercomputing facilities. F. Pichierri thanks the Graduate School of Engineering and the Global COE program of Tohoku University for financial support.

Supporting Information Available: Cartesian coordinates of the nine Zn-CNT heterojunctions investigated in this work and their corresponding *I*−*V* curves as well as their total transmission spectra. This material is available free of charge *via* the Internet at http://pubs.acs.org.

REFERENCES AND NOTES

1. Mieszawska, A. J.; Jalilian, R.; Sumanasekera, G. U.; Zamborini, F. P. The Synthesis and Fabrication of One-Dimensional Nanoscale Heterojunctions. *Small* **2007**, *3*, 722–756.
2. Datta, S. Quantum Transport: Atom to Transistor; Cambridge University Press: Cambridge, 2005.
3. Pichierri, F.; Khazaei, M.; Kawazoe, Y. Quantum-Chemical Design of Covalent Linkages for Interconnecting Carbon Nanotubes. *Mater. Trans.* **2007**, *48*, 2148–2151.
4. Khazaei, M.; Lee, S. U.; Pichierri, F.; Kawazoe, Y. Computational Design of a Rectifying Diode Made by Interconnecting Carbon Nanotubes with Peptide linkages. *J. Phys. Chem. C* **2007**, *111*, 12175–12180.
5. Hirsch, A. Functionalization of Single-Walled Carbon Nanotubes. *Angew. Chem., Int. Ed.* **2002**, *41*, 1853–1858.
6. Sinnott, S. B. Chemical Functionalization of Carbon Nanotubes. *J. Nanosci. Nanotechnol.* **2002**, *2*, 113–123.
7. Balasubramanian, K,; Burghard, M. Chemically Functionalized Carbon Nanotubes. *Small* **2005**, *1*, 180–192.
8. Pichierri, F. Nanosoldering of Thia-cucurbituril Macrocycles with Transition Metals Affords Novel Tubular Nanostructures: A Computational Study. *Chem. Phys. Lett.* **2005**, *403*, 252–256.
9. Greenwood, N. N., Earnshaw, A. Chemistry of the Elements; Butterworth-Heinemann: Oxford, 1998.
10. Wardell, J. L. Organometallic Compounds of Zinc, Cadmium, and Mercury; Chapman and Hall: London, 1985.
11. Stokbro, K.; Taylor, J.; Brandbyge, M.; Mozos, J. -L.; Ordejon, P. Theoretical Study of the Nonlinear Conductance of Di-thiol Benzene Coupled to Au(111) Surfaces via Thiol and Thiolate Bonds. *Comput. Mater. Sci.* **2003**, *27*, 151–160.
12. Kaun, C. -C.; Guo, H.; Grutter, P.; Lennox, R. B. Momentum Filtering Effect in Molecular Wires. *Phys. Rev. B* **2004**, *70*, 195309.
13. Clarke, D. R. Varistor Ceramics. *J. Am. Ceram. Soc.* **1999**, *82*, 485–502.
14. Perdew, J. P. Generalized Gradient Approximations for Exchange and Correlation: A Look Backward and Forward. *Physica B* **1991**, *172*, 1–6.
15. Kresse, G.; Furthmüller, J. Efficiency of *Ab-initio* Total Energy Calculations for Metals and Semiconductors Using a Plane-Wave Basis Set. *Comput. Mater. Sci.* **1996**, *6*, 15–50.
16. Perdew, J. P.; Burke, K.; Ernzerhof, M. Generalized Gradient Approximation Made Simple. *Phys. Rev. Lett.* **1996**, *77*, 3865–3868.
17. Troullier, N.; Martins, J. L. Efficient Pseudopotentials for Plane-Wave Calculations. II. Operators for Fast Iterative Diagonalization. *Phys. Rev. B* **1991**, *43*, 8861–8869.
18. Mozos, J. L.; Ordejon, P.; Brandbyge, M.; Taylor, J.; Stokbro, K. Simulations of Quantum Transport in Nanoscale Systems: Application to Atomic Gold and Silver Wires. *Nanotechnology* **2005**, *13*, 346–351.
19. Brandbyge, M.; Mozos, J. L.; Ordejon, P.; Taylor, J.; Stokbro, K. Density-Functional Method for Nonequilibrium Electron Transport. *Phys. Rev. B* **2002**, *65*, 165401.